Improved Fatigue Performance of Friction Stir Welds with Low Plasticity Burnishing: Residual Stress Design and Fatigue Performance Assessment

Paul Prevéy
Lambda Research, 5521 Fair Lane, Cincinnati, OH 45227 US

Murray Mahoney
Rockwell Scientific, 1049 Camino dos Rios, Thousand Oaks, CA 91360 US

Keywords: friction stir welds, residual stress, low plasticity burnishing, LPB, fatigue, pitting corrosion, corrosion fatigue, surface enhancement.

Abstract

Although friction stir welding (FSW) produces minimal distortion, residual stresses are created that impact fatigue and stress corrosion performance. X-ray diffraction residual stress and cold work mapping methods used at Lambda Research for FSW studies are described. Post weld surface enhancement processing can be used to place the FSW region in compression to improve fatigue performance. Deep compressive residual stress distributions produced by low plasticity burnishing (LPB) designed to improve fatigue and corrosion fatigue performance in aluminum alloy FSW are described. The LPB tooling and FSW processing are presented. Corrosion fatigue testing used for FSW samples is described and compared to fracture mechanics based fatigue life predictions calculated for the measured residual stress distributions. Residual stress and corrosion fatigue results for aluminum alloy 2219-T8751 are presented.

Introduction

FSW produces a distribution of tensile residual stress throughout the stir zone, maximized at the boundary with the heat affected zone (HAZ).[1,2] Corrosion pitting and stress corrosion cracking have been associated with stir zone tension. The fatigue strength reduction caused by salt pit corrosion is well established for both steels[3] and aluminum alloys[4], and typically reduces the endurance limit by half. LPB[5-8] is a surface enhancement technology demonstrated to provide a surface layer of deep high magnitude residual compression sufficient to effectively eliminate the corrosion fatigue debit.[9-11] LPB tooling can be designed to process the weld surface during the FSW operation, producing a FSW of superior fatigue strength and surface finish. This paper provides a brief overview of the residual stress distributions, corrosion fatigue strength of FSW with and without LPB, and summarizes the stress measurement and fatigue testing methods.

Experimental Technique

LPB of FSW: LPB is a method of CNC controlled burnishing designed to produce a deep layer of highly compressive residual stress with a minimum amount of cold working, or plastic deformation.[5-8] Residual compressive stresses approaching the material yield strength are developed using a series of passes of a freely rotating ball tool producing an accumulated plastic strain, or cold work, level of less than 3 to 5%. In contrast, the multiple random shot impacts of conventional shot peening produce cold work levels ranging from 20% to over 100%, leaving a severely deformed surface layer with a high dislocation density that adversely affects the thermal and mechanical stability of the compressive layer. [5,7]

Unlike LPB, conventional roller and ball burnishing utilize a hard wheel tool or fixed lubricated ball pressed into the surface of an axisymmetric work piece with sufficient force to deform the near surface layers, usually in a lathe. Burnishing is performed with multiple passes, often under increasing load, to improve surface finish and to deliberately cold work the surface. Roller and ball burnishing have been studied in Russia and Japan, and were applied most extensively in the USSR in the 1970's. Various burnishing methods are used, particularly in

Proceedings Thermec 2003
Madrid, Spain, July 7-11, 2003

Eastern Europe to improve fatigue life. Improvements in high cycle fatigue, corrosion-fatigue, and stress corrosion cracking are documented, with fatigue strength enhancement attributed to improved finish, the development of a compressive surface layer, and the increased yield strength of the cold worked surface.[12-17] Optimum forces and rolling parameters were established to minimize roughness and/or maximize surface hardening [18-21]. Analytical models to predict the residual stresses have been attempted in England [22] and France. [23] "Deep rolling" employs either roller tools or a partially hydrostatically supported burnishing ball, but differs from LPB in the use of higher loads and cold work levels, tool design and control. X-ray diffraction line broadening and micro-hardness reveal that deep rolling produces even more cold work than shot peening. [24-26]

The basic LPB tool is comprised of a ball that is supported in a spherical hydrostatic bearing as shown in Fig. 1. The tool can be held in any CNC lathe or mill, or may be incorporated into a fusion welding or FSW apparatus. A fluid, even machining coolant, is used to pressurize the bearing with a continuous flow to support the ball. The ball does not contact the bearing seat, even under load. The ball is loaded normal to the surface of a component with a hydraulic cylinder that is in the body of the tool. LPB can be performed in conjunction with chip forming machining operations or FSW in the same CNC machine tool. The ball rolls across the surface of a component in a pattern defined in the CNC code, as in any machining operation. The tool path and normal pressure applied are designed to create a distribution of compressive residual stress. The form of the compressive residual stress distribution is designed to counter applied stresses and optimize fatigue or stress corrosion performance. With no shear forces acting on the ball, it is free to roll in any direction. As the ball rolls over the component, the pressure from the ball plastically deforms the surface of the material under the ball by a controlled amount, leaving a zone of compression in the burnished area. No material is removed during the process. The surface is permanently displaced inward by only a few ten-thousandths of an inch (.0001- .0006 in. (0.0025-0.0152 mm)). LPB smoothes surface asperities leaving an improved surface finish that can be better than 5 µin., RA.

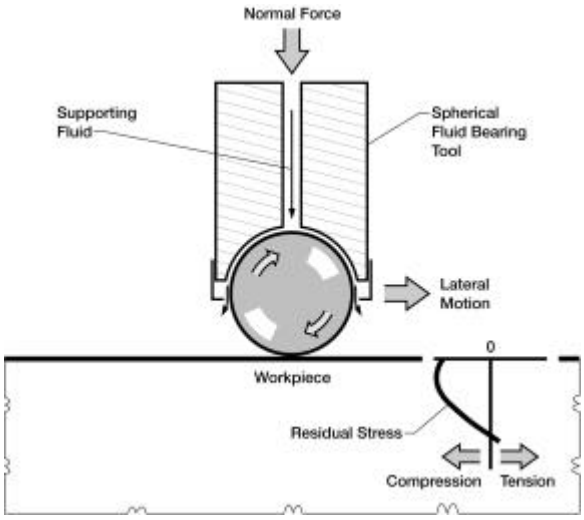

Fig. 1: LPB Schematic

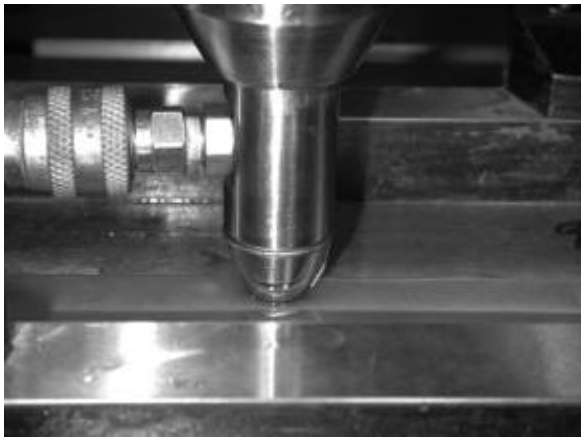

Fig. 2: Photo of FSW plate being low plasticity burnished with single ball tool.

Fig. 2 shows the laboratory apparatus used in this investigation for LPB processing of FSW samples in a CNC controlled vertical milling machine. The processing parameters are developed empirically using x-ray diffraction measurement of the residual stress distribution to adjust the ball size, material, pressure, and feed until suitable depth and magnitude of compression are achieved. Details of the LPB parameter development procedure are beyond the scope of this paper.

Material: The FSW samples used in this study were fabricated from 2219-T8751 aluminum plates with nominal composition

6.3Cu – 0.3Mn – 0.2Si – 0.3Fe – 0.1Zn - 0.02Mg – 0.06Ti – remainder Al, prepared by Rockwell Scientific. The FSW processing has been described previously.[1] Nominal dimensions of the plates were 914 (length) x 152 (width) x 9.5mm (thick). The plates contained a single weld in the center down the 914 mm length.

High Cycle Fatigue Testing

High cycle fatigue (HCF) testing was performed at 30 Hz and R= S_{min}/S_{max}=0.1 under cyclic constant stress amplitude at ambient temperature in four-point bending. A photo of an LPB processed FSW sample positioned in the fatigue test apparatus is shown in Fig. 3. The HCF sample was designed with a trapezoidal cross-section to force fatigue failures to initiate in the compressive gage section. The sample features 30-deg. sloping sides, allowing the gage section to be LPB processed across the upper surface and down the sides to below the neutral axis in bending to force fatigue initiation at the top surface of the gage section.

All HCF samples were milled on the weld side prior to either LPB or salt fog exposure to remove the weld flash and circular tooling marks left by the FSW process. The weld flash was milled flush with the parent metal. Only the weld side of the sample was LPB processed over a 50 mm (2.0-in) wide zone centered on the weld, which included the HAZ. Rockwell hardness measurements were across the surface to document the work hardening/softening produced by FSW. A total of four fatigue S-N curves were generated from the conditions given in Table 1.

Group No.	Group Identification
1	FSW + Milled
2	FSW + Milled + LPB
3	FSW + Milled + 100 hr. Salt Exposure
4	FSW + Milled + LPB + 100 hr. Salt Exposure

Table 1

Corrosion exposure prior to fatigue testing was conducted in 5wt% NaCl solution fog at a temperature of 95F for 100 hrs. in a Singleton Salt Fog Cabinet in accordance with ASTM B117-97. Fractography was performed initially optically at magnifications up to 40X to identify and locate fatigue origins, which were then recorded with a Nikon 990 digital camera and stereoscope microscope at 15X.

Fatigue Modeling: Fatigue life-prediction modeling analysis was performed using the fracture mechanics based code AFGROW. A semi-circular starting surface crack of 100 microns (0.004 in.) was assumed for untreated specimens. HCF performance for salt fog pitted samples was predicted assuming an initial pit of 500µm (0.02 in.) depth. The HCF specimen was modeled as a simple rectangular cross-section under pure four-bending. Full S-N curves were predicted and compared with actual data for the tested specimens.

Residual Stress Measurements: XRD residual stress measurements were made employing a $\sin^2\psi$ technique and the diffraction of chromium $K\alpha_1$ radiation from the (311) planes of the 2219-T8751 alloy, after verifying that the lattice spacing was a linear function of $\sin^2\psi$ as required for the plane stress linear elastic residual stress model.[27-30] The samples were rocked through an angular range of ±1.5º around the mean psi angles during measurement to integrate the diffracted intensity over more grains in order to minimize the influence of the grain size. The value of the x-ray elastic constants required to calculate the macroscopic residual stress from the strain normal to the (311) planes of the 2219-T8751 were determined in accordance with ASTM E1426-91.[31] Systematic errors were monitored per ASTM specification E915.

Residual stress distributions were measured using an automated translation device, capable of collecting a large volume of measurements in a relatively small amount of time, with minimal technician interaction shown in Fig. 4.[32] The computer controlled translation stage allows motion in the three principal axes to accurately locate the sample surface and measurement location. X-ray diffraction residual stress measurements were made at the weld surface, and half-thickness, to document the stress distribution through the stir zone. Measurements were made parallel and perpendicular to the weld-line and as a function of distance from the weld center in ~2.5mm (~0.01 in.) steps. Electropolishing was used to remove layers for subsurface measurement. The residual stress measurements were corrected for both the penetration of the radiation into the subsurface stress gradient[33] and for stress relaxation caused by layer removal using both

the closed form solutions of Moore and Evans[34] and finite element based solutions.

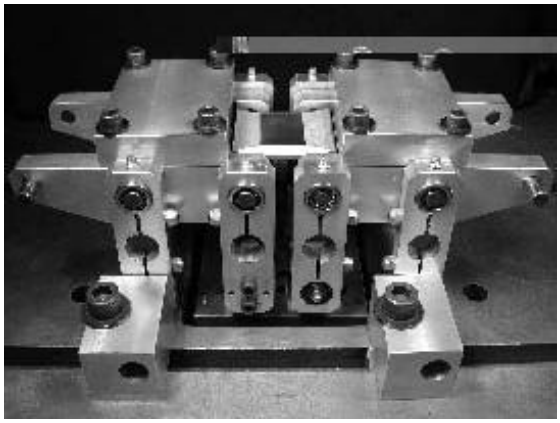

Fig. 3: Photo of LPB FSW fatigue specimen in 4-point bend fatigue fixture. The LPB zone is evident as the central region of improved surface finish.

Fig. 4: Automated x-ray diffraction residual stress measurement apparatus with FSW mounted for residual stress mapping.

RESULTS AND DISCUSSION

Residual Stresses: Residual stress distributions both parallel and perpendicular to the weld line are presented in Fig. 5a and 5b, for the top surface and mid-thickness of the FSW. Residual stress data are presented as functions of depth and distance from the weld centerline for both the as-welded condition and after LPB processing. Compressive stresses are shown as negative values and tensile as positive.

At the weld surface, the FSW process produces tension parallel to the weld line and compression in the perpendicular orientation. Maximum surface tension on the order of 100 MPa (15 ksi) occurs at the edges of the stir zone. LPB introduces compression in all directions, ranging from –180 MPa (-26 ksi) in the perpendicular to -500 MPa (-73 ksi) in the parallel direction. The highest tension occurs at half-thickness, approaching +200 MPa (29 ksi) parallel to the weld line, considerably higher than previously reported where measurements were taken only near the crown[35] or on the top and bottom surfaces.[2] At this depth, over 4mm (0.16 in.) below the surface, the material is not deformed by the LPB processing used in this study, and the residual stresses at half-thickness are essentially identical in as welded and LPB samples. Residual stresses perpendicular to the weld direction are quite low due to the lack of constraint perpendicular to the weld line.

The variation in working of the alloy through the stir zone and into the HAZ produced a variation in hardness. The yield strength, although not measured here, presumably varies accordingly. The hardness variation shown in Fig. 6 as a function of distance from the weld center indicates softened material in the stir zone, with the softest material at the edges of the stir zone boundaries. No attempt was made to adjust the burnishing pressure for the change in yield strength across the stir zone. In the softer HAZ and stir zones, the material response to LPB would be different than in the higher yield stress weld zone and parent metal. Variation of processing to account for the variation in yield strength, or to deliberately cold work the material to restore yield strength, are possible during LPB post weld processing, but were not attempted in this study.

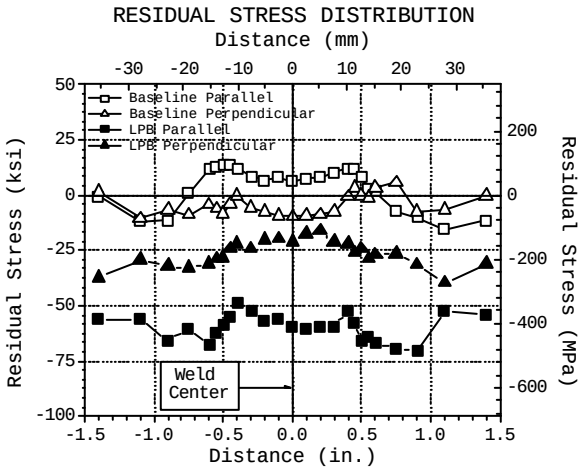

(a)

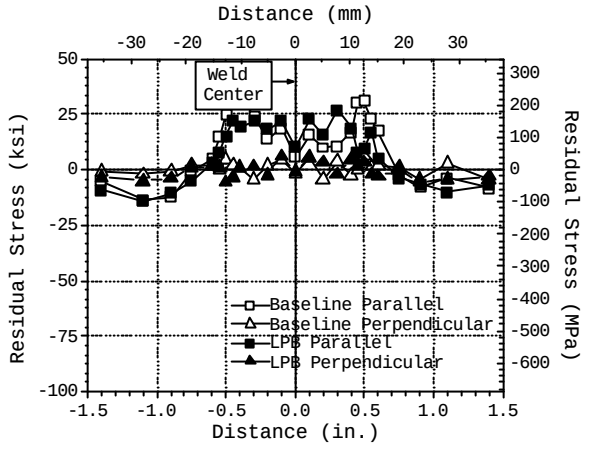

(b)

Fig. 5: Residual stress parallel and perpendicular to the weld line in FSW 2219-T8751 with and without LPB, (a) weld surface, (b) half-thickness.

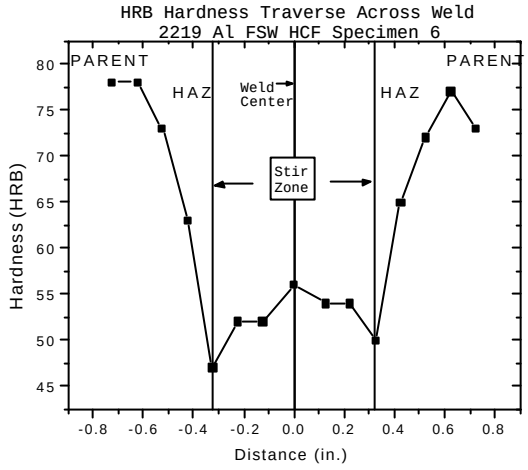

Fig. 6: Surface hardness (HRB) traverse across the FSW showing softened weld material.

Fatigue and Corrosion Fatigue: High cycle fatigue results are presented in Fig. 8 for the different test conditions. With the FSW flash and tool marks removed by milling, the endurance limit was nominally 230MPa. (33 ksi) Salt fog pitting exposure for 100 hr. reduced the endurance limit nominally 25%. LPB increased the endurance limit to 300MPa (44 ksi), with or without pitting. Salt fog exposure had no measurable affect upon the fatigue strength of the previously LPB processed FSW.

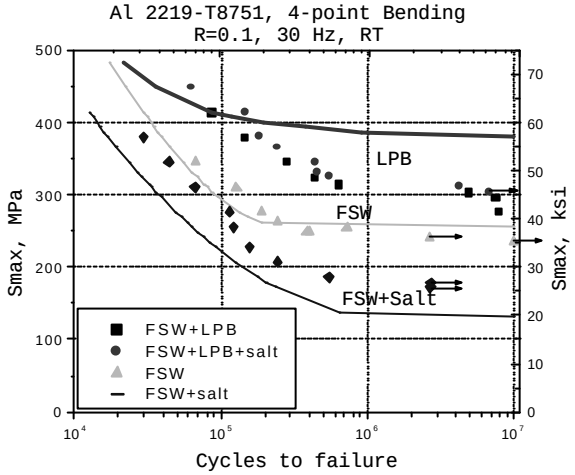

Fig. 7: Fatigue and corrosion fatigue test results for FSW 2219-T8751 aluminum with and without LPB. AFGROW predicted fatigue performance for the measured residual stress distributions is shown as solid lines.

Fatigue initiation sites for the FSW specimens were typically at the milled surface within the gage region. The higher applied stresses produced multiple initiations within the gage region. Almost all the fatigue initiation sites were outside of the sir zone. At both low and high stress, LPB forced the fatigue initiation subsurface, below the highly compressive layer. Presumably, an applied stress even higher than that producing subsurface failure would be required to initiate failure from the compressive surface. The corroded samples exhibited more multiple initiation sites at numerous corrosion pits. Fatigue initiation was again subsurface for LPB processed samples from the corner, and not from the corrosion pits. LPB was effective in preventing the corrosion pits from acting as fatigue initiation sites.

Fatigue Modeling: Fig. 8 includes HCF S-N curves generated using the AFGROW code for life prediction analysis. The curves are calculated in each case for the residual stress distribution and flaw size measured for each condition. For the FSW and FSW + Salt, the predicted performance is in good agreement with the test results. The conservative prediction for the FSW samples is attributed to the

existence of a starting crack/notch size less severe than that assumed in the model, while for the FSW+100 hrs salt exposed condition the assumed starting pit size appears to predict fatigue life satisfactorily.

The predictions for LPB treated specimens were consistently higher than the test results, with or without salt fog pitting. The prediction for LPB alone was so high that it is not included in Fig. 7. The LPB + Salt exposure prediction, which assumes failure from the surface imperfections, is clearly higher than the test results, which are entirely subsurface at the lower stress levels needed for initiation. The surface failure model assumed simply does not apply for subsurface failure. LPB processed specimens generally failed from sub-surface crack initiation, thus making the effect of corrosion irrelevant in the analysis. A more accurate life-prediction methodology incorporating subsurface cracking mechanisms is needed to fully and more accurately predict fatigue life.

Conclusions

Automated X-ray diffraction mapping can be used to document the residual stress distributions parallel and perpendicular to the weld line through the thickness of FSW. FSW of 2219-T8751 9.5mm (0.20 in.) plate produces tensile residual stresses both at the top (tool shoulder contact) surface and in the interior of the stir zone. Maximum tension exceeding +200 MPa (29 ksi) in the direction parallel to the weld line occurs in the interior at the stir zone-HAZ boundary, and is nominally symmetrical with respect to the advancing and retreating sides. LPB post weld processing left the surface of the FSW specimen in compression, on the order of –450 MPa (-58 ksi), in all directions.

Four-point bend fatigue testing can be used with and without prior salt fog pitting corrosion to assess the fatigue performance of FSW in the laboratory. Initiation sites correspond to the regions of tension at the stir zone-HAZ boundaries. LPB post weld processing nearly doubles the fatigue strength of 2219-T8751 FSW exposed to pitting corrosion. The layer of compressive residual stress produced by LPB eliminates fatigue initiation from corrosion pits, restoring the strength of the weld to more than the un-corroded strength.

Acknowledgement

The authors gratefully acknowledge Boeing for financial support.

References

1. D. Hornbach, M. Mahoney, P. Prevéy, D. Waldron and J. Cammett, ”Low Plasticity Burnishing of Friction Stir Welds in 2219 Aluminum to Increase Corrosion Fatigue Life”, Proceedings Pine Mountain Conference, (2002).
2. C. DalleDonne, E. Lima, J. Wegener, A. Pyzalla and T. Buslaps, “Investigations of Residual Stresses in Friction Stir Welds”, 3rh Int. Symposium on Friction Stir Welding, (2001), TWI (UK)
3. ASM Handbook, Vol. 19, *Fatigue and Fracture*, pp. 596-597, S.R. Lampman, ed., ASM International, Metals Park, OH (1996).
4. N.E. Dowling, *Mechanical Behavior of Materials*, p. 365, Prentice Hall, NJ, (1993).
5. U.S. Patents 5,826,453 (Oct. 1998), 6,415,486 B1 (Jul. 2002) other US and foreign patents pending.
6. “Low Plasticity Burnishing”, *NASA Tech Briefs*, Aug. 2002, pg. 50.
7. “Longer Life with Low-Plasticity Burnishing”, *Manufacturing Engineering*, SME, ed. Brian Hogan, Dec. 2001, pg. 34-38.
8. T. Gabb, J. Telesman, P. Kantzos, P. Prevéy, “Surface Enhancement of Metallic Materials”, *Advanced Materials & Processes*, ASM, ed. Peg Hunt, Jan. 2002, pg. 69-72.
9. J. Cammett and P. Prevéy, “*Low Cost Corrosion Damage Mitigation and Improved Fatigue Performance of Low Plasticity Burnished 7075-T6*,” Proc. 4th International Aircraft Corrosion Workshop, Solomons, MD, Aug. 22-25, (2000).
10. J. Cammett and P. Prevéy, “*Fatigue Strength Restoration in Corrosion Pitted 4340 Alloy Steel via Low Plasticity Burnishing*,” Retrieved Aug. 30, 2002, from http://www.lambda-research.com/publics.htm.
11. P. Prevéy and J. Cammett, “*The Influence of Surface Enhancement by Low Plasticity Burnishing on the Corrosion Fatigue Performance of AA7075-T6*,” Proc. 5th International Aircraft Corrosion Workshop, Solomons, MD, Aug. 20-23, (2002).

12. V.V. Belozerov, et al., (1986), Met. Sci. Heat Treat., 28, No. 7-8, pp. 565-569.
13. V.T. Stepurenko, et al., (1976), Protection of Metals, 12, No. 4, pp. 386-389.
14. D.D. Papshev, Yu G. Golubev, (1972), Russian Engineering Journal, 52, No. 4, pp. 48-51.
15. M. Kh. Freid, et al., (1994), Protection of Metals, 20, No. 2, pp. 263-265.
16. L.M. Belkin, et al, (1984), Soviet Engineering Research, 4, No. 9, pp. 30-32.
17. L.M. Belkin, (1983), Soviet Materials Science, 19, No. 3, pp. 225-228.
18. M. Fattouh, et al., (1988), Wear, 127, pp. 123-137.
19. N.H. Loh, et al., (1989), Wear 129, No. 2, pp. 235-243.
20. N.H. Loh, et al., (1993), Precision Engineering, 15, No. 2, pp. 100-105.
21. B. Kotiveerachari, R.L. Murty, (1985), International Journal of Production Research, 23, No. 3, pp. 499-521.
22. D.A. Hills, et al., (1979), Proc. Int'l Conference Wear of Materials, ASME, New York, NY, pp. 396-402.
23. S. Braham, J. Frelat, (1993), Proc. Computer Methods and Exp. Meas. for Surface Treatment Effects, Computational Mechanics Publications, Southampton, U.K., pp. 255-264.
24. W. Zinn and B. Scholtes, "Mechanical Surface Treatments of Lightweight Materials - Effects on Fatigue Strength and Near-Surface Microstructures," Journal of Materials Engineering and Performance, Volume 8(2), April 1999, pp. 145-151.
25. I. Altenberger, et.al., "Cyclic Deformation and Near Surface Microstructures of Shot Peened or Deep Rolled Austenitic Stainless Steel AISI 304," Materials Science and Engineering, A264, 1999, pp. 1-16.
26. A. Drechsler, et.al., "Mechanical Surface Treatments of Ti-10V-2Fe-3Al for Improved Fatigue Resistance", Materials Science and Engineering, A243, 1998, pp. 217-220.
27. Hilley, M.E. ed.,(1971), Residual Stress Measurement by X-Ray Diffraction, *SAE J784a*, (Warrendale, PA: Society of Auto. Eng.).
28. Noyan, I.C. and Cohen, J.B., (1987) Residual Stress Measurement by Diffraction and Interpretation, (New York, NY: Springer-Verlag).
29. Cullity, B.D., (1978) Elements of X-ray Diffraction, 2nd ed., (Reading, MA: Addison-Wesley), pp. 447-476.
30. Prevéy, P.S., (1986), "X-Ray Diffraction Residual Stress Techniques," *Metals Handbook*, 10, (Metals Park, OH: ASM), pp 380-392.
31. Prevéy, P.S., (1977), "A Method of Determining Elastic Properties of Alloys in Selected Crystallographic Directions for X-Ray Diffraction Residual Stress Measurement," Adv. In X-Ray Analysis, 20, (New York, NY: Plenum Press, 1977), pp 345-354.
32. *Diffraction Notes*, Residual Stress Contour Mapping, No. 19, Lambda Research, Cincinnati, OH, Summer (1997).
33. D.P. Koistinen and R.E. Marburger, *Transactions of the ASM*, **67** (1964).
34. M.G. Moore and W.P. Evans, "*Mathematical Correction for Stress in Removed Layers in X-ray Diffraction Residual Stress Analysis*," *SAE Transactions*, **66**, p 340-345, (1958).
35. M. James, M. Mahoney and D. Waldron, Proc. 1st International Symposium on Friction Stir Welding, Rockwell Science Center, T.O., CA, Pub. By TWI, June 14-16, (1999)